Chen, Min; Shi, Junjie; Taskinen, Pekka; Jokilaakso, Ari

Phase equilibria of the CaO–SiO2–TiO2–Al2O3–MgO system in air at 1250–1400 °C

Published in:
Ceramics International

DOI:
10.1016/j.ceramint.2020.07.268

Published: 01/12/2020

Document Version
Peer-reviewed accepted author manuscript, also known as Final accepted manuscript or Post-print

Please cite the original version:
Chen, M., Shi, J., Taskinen, P., & Jokilaakso, A. (2020). Phase equilibria of the CaO–SiO2–TiO2–Al2O3–MgO system in air at 1250–1400 °C. *Ceramics International*, *46*(17), 27702-27710.
https://doi.org/10.1016/j.ceramint.2020.07.268

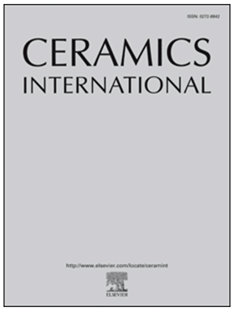

Phase equilibria of the CaO–SiO_2–TiO_2–Al_2O_3–MgO system in air at 1250–1400 °C

Min Chen, Junjie Shi, Pekka Taskinen, Ari Jokilaakso

PII: S0272-8842(20)32285-9
DOI: https://doi.org/10.1016/j.ceramint.2020.07.268
Reference: CERI 26022

To appear in: *Ceramics International*

Received Date: 3 June 2020
Revised Date: 7 July 2020
Accepted Date: 27 July 2020

Please cite this article as: M. Chen, J. Shi, P. Taskinen, A. Jokilaakso, Phase equilibria of the CaO–SiO_2–TiO_2–Al_2O_3–MgO system in air at 1250–1400 °C, *Ceramics International* (2020), doi: https://doi.org/10.1016/j.ceramint.2020.07.268.

Phase equilibria of the CaO-SiO_2-TiO_2-Al_2O_3-MgO system in air at 1250-1400 °C

Min Chen[1], Junjie Shi[1*], Pekka Taskinen[1], Ari Jokilaakso[1]

[1]Department of Chemical and Metallurgical Engineering, School of Chemical Engineering, Aalto University,
Kemistintie 1F, P.O. Box 16100, FI-00076 Aalto, Finland

Email address for all authors:

Min Chen, minchen0901@hotmail.com

Junjie Shi*, Corresponding author, junjie.shi@aalto.fi; junjieshi@126.com

Pekka Taskinen, pekka.taskinen@aalto.fi

Ari Jokilaakso, ari.jokilaakso@aalto.fi

Declarations of interest: none.

ORCID:

Min Chen, https://orcid.org/0000-0003-0544-4359

Junjie Shi, https://orcid.org/0000-0002-8673-0404

Pekka Taskinen, http://orcid.org/0000-0002-4054-952X

Ari Jokilaakso, http://orcid.org/0000-0003-0582-7181

Abstract

The equilibrium phase relations of the CaO-SiO_2-TiO_2-Al_2O_3-MgO system were investigated experimentally in air at 1250-1400 °C using a high-temperature equilibration/quenching technique, followed by direct phase analysis by scanning electron microscopy equipped with X-ray energy dispersive spectroscopy. The equilibrium solid phases of silica, rutile, and pseudobrookite solid solution were found to coexist with the liquid phase. The 1300-1400 °C isothermal sections were constructed based on the experimentally measured liquid compositions. The experimental results were compared with simulations using MTDATA and FactSage thermodynamic software and their databases. This study provides guidelines for the selective crystallization of pseudobrookite from titania-bearing slag.

Keywords: Phase equilibria; thermodynamic; titania-bearing slag; liquidus temperature; circular economy

1. Introduction

Titania-bearing slag is a typical industrial byproduct of the blast furnace smelting of vanadium and titanium magnetites [1], where the TiO_2 content is approximately 22-25 wt% [2-4] and indicates a good source of titania. With a greater demand for a circular economy, various techniques, such as selective crystallization of TiO_2-rich crystals followed by phase separation (SCPS), hydrometallurgical acid leaching, and the melting reduction method [5-12], have been developed so far for effective recovery of the titania values from titania-bearing slags. Of these, the SCPS method was suggested to have the most industrial potential for slag processing [13].

The components of titania-bearing slags in air can be described by the CaO-SiO_2-TiO_2-Al_2O_3-MgO system [13, 14]. Rutile, perovskite, and pseudobrookite are the main TiO_2-rich mineral phases in the system. The selective enrichment of TiO_2 into perovskite has been extensively investigated by many researchers [3, 15-24], but limited efforts have been devoted to the crystallization of rutile and pseudobrookite [3, 9, 12, 25]. Compared with the mineral phases of rutile and pseudobrookite, the low theoretical content of TiO_2 in perovskite, approximately 58 wt%, as well as its dendrite structure and similar density to other phases, suggest that perovskite is not an ideal choice for recovering titania from Ti-bearing slags [9]. In contrast, pseudobrookite has the advantages of a high theoretical TiO_2 content (more than 70%) and higher density (4.19 g cm^{-3}) than that of the glass phase (2.8 g cm^{-3}) [3]. Therefore, it is appropriate to enrich the TiO_2 into the pseudobrookite phase. To obtain further information about the precipitation conditions of pseudobrookite in slag, it is essential to characterize the pseudobrookite primary phase field in the CaO-SiO_2-TiO_2-Al_2O_3-MgO system by constructing a detailed phase diagram.

Goso et al. [14] obtained the phase equilibria and liquidus surface of the 19.69 wt% SiO_2-37.19 wt% TiO_2-13.12 wt% Al_2O_3-30.00 wt% (CaO+MgO) system at P_{O2} of 10^{-16} to 0.21 atm using FactSage simulation. The spinel solution ((Mg)(Al, Ti)O_4) was found to precipitate as the primary phase with higher MgO content, whereas the crystallization of pseudobrookite solution ($MgTi_2O_5$-Al_2TiO_5) took place when the P_{O2} ranged between 10^{-10} and 10^{-15} atm. Wang et al. [26] investigated the phase equilibria of the CaO-SiO_2-TiO_2-Al_2O_3-MgO system with constant 10 wt% Al_2O_3 and 5 wt% MgO at 1500 °C. The primary phase field of anosovite (i.e., the pseudobrookite solid solution in the present study) in the TiO_2-rich corner was obtained. The phase relations of the CaO-SiO_2-TiO_2-Al_2O_3-MgO system with fixed 5-10 wt% MgO and 10-30 wt% Al_2O_3 at 1250-1500 °C were systematically studied by Shi et al. [27-32] and Sun et al. [33-35]. They paid a lot of attention to the perovskite primary phase field. However, the TiO_2-enriched pseudobrookite solid solution ($MgO\cdot 2TiO_2$, $Al_2O_3\cdot TiO_2)_{ss}$) was observed in only a limited number of studies [27-30]. Osborn et al. [36] investigated the liquidus temperatures of the CaO-MgO-Al_2O_3-TiO_2-SiO_2 system on different Al_2O_3-TiO_2 levels: 10 wt% Al_2O_3-2.5 wt% TiO_2, 10 wt% Al_2O_3-5 wt% TiO_2, 10 wt% Al_2O_3-10 wt% TiO_2, and 15 wt% Al_2O_3-2.5 wt%TiO_2. Zhao et al. [37] studied the TiO_2-CaO-MgO-Al_2O_3-SiO_2 system with fixed (CaO/MgO) and (Al_2O_3/SiO_2) ratios at carbon saturation. The isotherms in the perovskite and pseudobrookite $(2(Ti^{3+}, Mg^{2+}, Al^{3+})\cdot Ti^{4+}O_5)$ primary phase fields were constructed in a TiO_2-(CaO+MgO)-(SiO_2+Al_2O_3) pseudo-ternary phase diagram.

Although the phase equilibria of the CaO-SiO_2-TiO_2-Al_2O_3-MgO system have been investigated to some extent, there remain many gaps and inconsistencies in the knowledge base about the phase relations of the system, and detailed composition ranges for the precipitation of pseudobrookite are far from sufficient. Therefore, this study was initiated with the focus on the phase equilibria of the CaO-SiO_2-TiO_2-Al_2O_3-MgO system at 1250-1400 °C in air. Based on the typical industrial composition of Ti-bearing slags [1, 2, 5], the Al_2O_3 and MgO contents in the initial slag mixtures were designed to be 15 wt% and 10 wt%, respectively. This study will provide useful information for the selective crystallization of the pseudobrookite phase.

2. Experimental

High purity powders of CaO (Sigma-Aldrich, 99.9 wt%), SiO_2 (Alfa Aesar, 99.995 wt%), Al_2O_3 (Sigma-Aldrich, 99.99 wt%), MgO (Alfa Aesar, 99.995 wt%), and TiO_2 (Sigma-Aldrich, 99.8 wt%) were used as starting materials. Each powder was weighed in a certain proportion, mixed thoroughly in an agate mortar, and then pressed into a pellet.

The high-temperature equilibration of the oxide mixtures was carried out in a vertical, impervious alumina tube furnace, as shown in Figure 1, followed by quenching in an ice-water mixture [38]. The furnace temperature was regulated using a Eurotherm 3216 PID controller with an uncertainty of ±3 °C. The sample pellet was placed in a crucible made of platinum foil and held in the center of the uniform temperature hot zone by a platinum wire from the top of the furnace. An alumina-shielded S-type Pt/Pt-10%Rh thermocouple placed next to the sample was employed for monitoring the sample temperature. The thermocouple was calibrated beforehand at the factory with a maximum deviation from standard of ±2 °C [39]. For each experiment, approximately 0.15 g of slag was equilibrated at the experimental temperature (1250-1400 °C) for at least 48 hours [27, 29, 40]. After equilibration, the samples were released, dropped under gravity, and were quenched in an ice-water mixture. Detailed information about the experimental furnace and procedures was provided in our previous study [40].

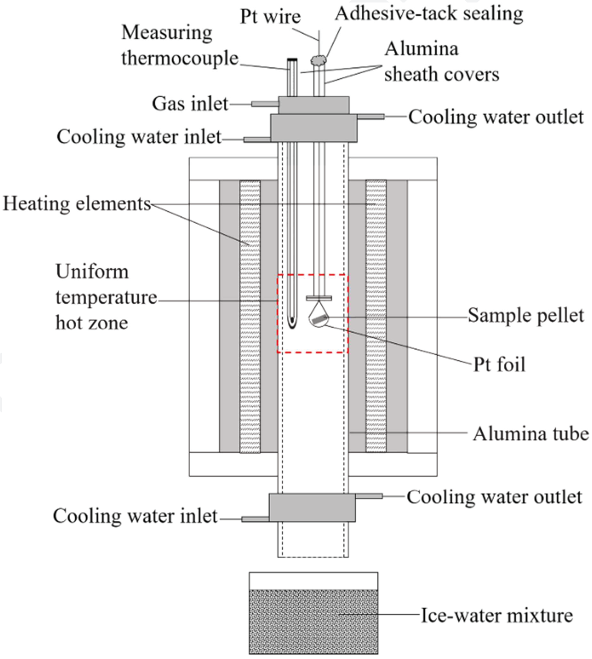

Fig. 1. Schematic cross-section of experimental furnace.

The quenched samples were dried at ambient temperature post quenching, mounted in epoxy resin, ground and polished using a metallographic polishing cloth with a diamond spray. The polished surfaces of the samples were carbon-coated to ensure good electrical conductivity. The equilibrium phase compositions were analyzed using a Tescan MIRA 3 scanning electron microscope (SEM, Tescan, Brno, Czech Republic) equipped with an UltraDry silicon drift energy dispersive X-ray spectrometer (EDS, Thermo Fisher Scientific, Waltham, MA, USA) and NSS microanalysis software. The analytical settings for SEM-EDS are an accelerating voltage of 15 kV, beam current of 20 nA, and working distance of 20 mm. The standards and analyzed X-ray lines in the EDS analysis were as follows: olivine (for O, Kα), quartz (for Si, Kα), metal Al (for Al, Kα), metal Mg (for Mg, Kα), calcite (for Ca, Kα), and metal Ti (for Ti, Kα). At least eight points were measured for each phase to ensure high statistical reliability. The Proza (Phi-Rho-Z) on-line matrix correction program [41] was employed for raw data processing before normalizing the results.

Table 1. Experimentally determined equilibrium phase compositions for the CaO-SiO_2-TiO_2-Al_2O_3-MgO system equilibrated with air ($P_{O2} = 10^{-0.6778}$ atm) at 1250-1400 °C.

Code	Temperature/°C	Initial composition/wt%					Equilibrium phases	Equilibrium composition/wt%				
		TiO_2	SiO_2	CaO	MgO	Al_2O_3		TiO_2	SiO_2	CaO	MgO	Al_2O_3
E1	1250	5.00	58.33	11.67	10.00	15.00	L	5.3(5) ± 0.37	61.5(8) ± 1.63	10.7(4) ± 0.11	7.8(0) ± 0.76	14.5(3) ± 0.45
							Silica	0.0(5) ± 0.05	99.9(5) ± 0.05	-	-	-
E3	1250	5.00	43.75	26.25	10.00	15.00	L	5.3(0) ± 0.12	47.7(3) ± 0.30	25.9(2) ± 0.13	7.4(5) ± 0.15	13.6(0) ± 0.18
E4	1250	15.00	50.00	10.00	10.00	15.00	L	10.0(2) ± 0.71	59.8(0) ± 2.52	9.8(1) ± 0.46	7.2(5) ± 0.58	13.1(2) ± 0.79
							Silica	0.0(2) ± 0.03	99.9(7) ± 0.03	-	-	-
							Rutile	99.0(5) ± 0.18	0.2(3) ± 0.04	0.2(5) ± 0.11	0.0(3) ± 0.02	0.4(4) ± 0.05
							Pseudobrookite	76.7(0) ± 0.25	0.4(2) ± 0.03	0.1(9) ± 0.06	17.2(0) ± 0.12	5.5(0) ± 0.32
E5	1250	15.00	42.86	17.14	10.00	15.00	L	15.3(8) ± 0.10	46.2(4) ± 0.06	16.8(7) ± 0.03	7.6(4) ± 0.07	13.8(7) ± 0.06
E6	1250	15.00	37.50	22.50	10.00	15.00	L	15.6(2) ± 0.12	41.5(3) ± 0.09	21.9(8) ± 0.07	7.1(5) ± 0.04	13.7(1) ± 0.13
E7	1250	25.00	41.67	8.33	10.00	15.00	L	10.7(2) ± 0.37	54.9(5) ± 0.31	10.7(9) ± 0.30	7.2(8) ± 0.46	16.2(6) ± 0.10
							Rutile	98.8(4) ± 0.16	0.2(7) ± 0.06	0.3(6) ± 0.10	0.0(3) ± 0.02	0.5(0) ± 0.04
							Pseudobrookite	74.9(6) ± 0.82	0.7(6) ± 0.73	0.3(2) ± 0.20	16.2(7) ± 0.43	7.6(8) ± 0.50
E13	1250	45.00	25.00	5.00	10.00	15.00	L	10.4(1) ± 0.05	54.4(6) ± 0.27	11.1(5) ± 0.04	4.9(8) ± 0.17	19.0(0) ± 0.42
							Rutile	98.9(2) ± 0.10	0.2(1) ± 0.04	0.2(0) ± 0.10	0.0(4) ± 0.02	0.6(4) ± 0.04
							Pseudobrookite	73.0(6) ± 0.82	0.4(6) ± 0.06	0.2(7) ± 0.10	14.7(2) ± 0.44	11.4(9) ± 1.19
E7	1300	25.00	41.67	8.33	10.00	15.00	L	14.2(3) ± 0.51	52.7(7) ± 0.89	10.8(1) ± 0.34	6.4(5) ± 0.11	15.7(3) ± 0.95
							Rutile	98.9(3) ± 0.18	0.2(5) ± 0.05	0.2(9) ± 0.14	0.0(3) ± 0.02	0.5(0) ± 0.04
							Pseudobrookite	76.1(6) ± 0.99	0.4(7) ± 0.04	0.2(0) ± 0.06	16.6(8) ± 0.45	6.4(9) ± 1.39
E8	1300	25.00	35.71	14.29	10.00	15.00	L	23.3(4) ± 0.12	39.7(7) ± 0.16	16.0(9) ± 0.04	7.1(5) ± 0.11	13.6(5) ± 0.06
E9	1300	25.00	31.25	18.75	10.00	15.00	L	25.4(2) ± 0.07	34.2(9) ± 0.20	19.2(5) ± 0.04	7.4(0) ± 0.10	13.6(5) ± 0.05
E10	1300	35.00	33.33	6.67	10.00	15.00	L	14.1(2) ± 0.15	52.1(8) ± 0.58	9.8(7) ± 0.08	7.5(1) ± 0.33	16.3(2) ± 0.31
							Rutile	98.9(8) ± 0.11	0.2(1) ± 0.03	0.1(6) ± 0.07	0.0(4) ± 0.02	0.6(1) ± 0.04
							Pseudobrookite	74.7(0) ± 0.19	0.4(7) ± 0.04	0.2(1) ± 0.05	15.7(8) ± 0.10	8.8(3) ± 0.21
E11	1300	35.00	28.57	11.43	10.00	15.00	L	22.4(9) ± 0.18	40.9(7) ± 0.16	15.2(7) ± 0.06	5.8(9) ± 0.15	15.3(9) ± 0.19
							Rutile	98.7(8) ± 0.16	0.2(5) ± 0.09	0.2(8) ± 0.11	0.0(5) ± 0.03	0.6(5) ± 0.05
							Pseudobrookite	74.1(3) ± 0.34	0.4(0) ± 0.03	0.2(4) ± 0.09	16.8(0) ± 0.22	8.4(2) ± 0.57
E12	1300	35.00	25.00	15.00	10.00	15.00	L	28.1(0) ± 0.18	32.5(8) ± 0.13	17.8(9) ± 0.08	6.2(5) ± 0.12	15.1(9) ± 0.10
							Rutile	98.9(9) ± 0.05	0.2(1) ± 0.02	0.1(9) ± 0.04	0.0(3) ± 0.01	0.5(8) ± 0.02
							Pseudobrookite	72.8(8) ± 0.50	0.4(0) ± 0.03	0.2(8) ± 0.08	16.2(3) ± 0.25	10.2(2) ± 0.71
E13	1300	45.00	25.00	5.00	10.00	15.00	L	13.0(6) ± 0.11	51.4(9) ± 0.25	10.1(9) ± 0.12	5.8(1) ± 0.04	19.4(4) ± 0.03
							Rutile	98.7(5) ± 0.11	0.2(2) ± 0.05	0.2(2) ± 0.06	0.0(3) ± 0.02	0.7(7) ± 0.03
							Pseudobrookite	70.2(2) ± 1.09	0.4(4) ± 0.02	0.1(5) ± 0.03	14.3(5) ± 0.63	14.8(3) ± 1.70
E13	1400	45.00	25.00	5.00	10.00	15.00	L	32.6(9) ± 0.23	37.4(8) ± 0.19	9.1(9) ± 0.17	4.4(4) ± 0.08	16.2(0) ± 0.13
							Pseudobrookite	74.3(0) ± 0.44	0.3(7) ± 0.04	0.0(7) ± 0.02	16.2(8) ± 0.23	8.9(8) ± 0.65
E14	1400	45.00	21.43	8.57	10.00	15.00	L	41.0(9) ± 0.18	25.5(8) ± 0.13	11.9(0) ± 0.08	6.8(8) ± 0.04	14.5(4) ± 0.09
E15	1400	45.00	18.75	11.25	10.00	15.00	L	43.1(7) ± 0.08	21.3(7) ± 0.06	13.7(3) ± 0.04	7.4(0) ± 0.08	14.3(3) ± 0.05
E16	1400	55.00	16.67	3.33	10.00	15.00	L	44.3(2) ± 0.18	28.4(5) ± 0.22	8.0(4) ± 0.20	3.3(9) ± 0.20	15.8(0) ± 0.10
							Rutile	98.9(5) ± 0.08	0.1(6) ± 0.02	0.0(5) ± 0.02	0.0(5) ± 0.02	0.8(0) ± 0.05
							Pseudobrookite	72.4(9) ± 0.45	0.3(5) ± 0.03	0.0(7) ± 0.01	15.2(6) ± 0.32	11.8(4) ± 0.76
E17	1400	55.00	14.29	5.71	10.00	15.00	L	46.9(5) ± 1.28	22.4(7) ± 1.01	11.1(1) ± 0.16	4.6(7) ± 0.19	14.7(9) ± 0.45
							Pseudobrookite	73.0(1) ± 0.46	0.3(8) ± 0.04	0.1(4) ± 0.05	15.0(9) ± 0.25	11.3(8) ± 0.68
E18	1400	55.00	12.50	7.50	10.00	15.00	L	47.5(2) ± 0.57	19.5(8) ± 0.48	12.6(8) ± 0.46	5.1(7) ± 0.30	15.0(6) ± 0.23
							Pseudobrookite	71.6(7) ± 0.57	0.4(1) ± 0.09	0.1(6) ± 0.06	15.0(8) ± 0.33	12.6(8) ± 0.83

3. Results and Discussion

The equilibrium phase compositions and typical microstructures of the samples obtained at 1250-1400 °C are shown in Table 1 and Figures 2-4, respectively. As the accuracy of EDS analysis is one decimal digit unit only, therefore, the second decimal digit was listed in the bracket. It should be noted that the designed slag compositions were not used for constructing the phase diagram so that the water contamination before the equilibration can be eliminated. Based on the prediction of the titanium oxide predominance phase diagram [40], titanium presented a valence state of Ti^{4+} in air, in the conditions of the present study. Therefore, the concentrations of titanium oxide were calculated from the EDS analyses and presented as TiO_2.

3.1 Phase relations at 1250-1400 °C

The equilibrium results at 1250 °C were more complicated compared with those at 1300 and 1400 °C. Single liquid phase domains and multiphase equilibria of two, three, and four phases were observed. Figures 2(a)-2(c) show typical microstructures of liquid-silica, homogeneous liquid, and liquid-rutile-pseudobrookite equilibria, respectively. A four-phase equilibrium, i.e., liquid-silica-rutile-pseudobrookite, was confirmed in sample E4 (Figure 2(d)). As the sample broke into tiny pieces in quenching, the three-phase equilibria of liquid-rutile-pseudobrookite and two-phase equilibria of liquid-silica were found in different parts of the sample, as shown in Figures 2(d1) and 2(d2), respectively, indicating that the primary phase fields of silica, rutile, and pseudobrookite are adjacent to each other.

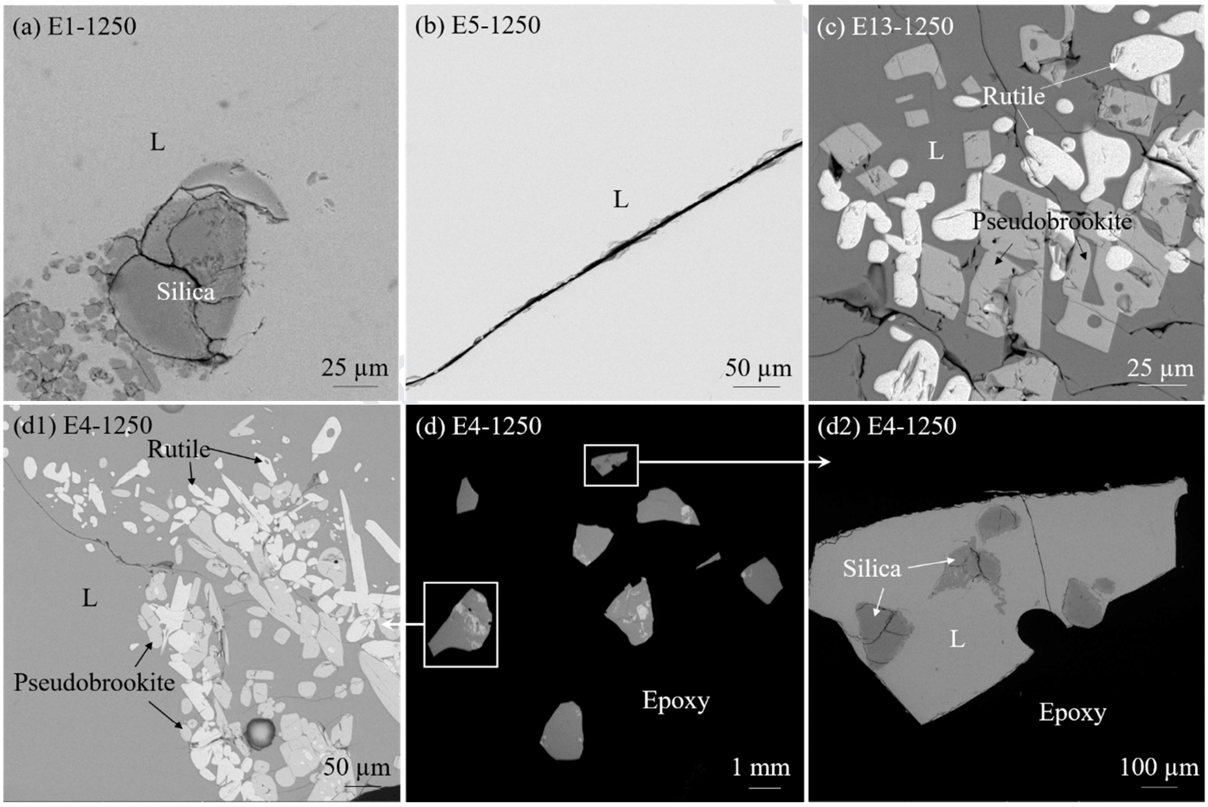

Fig. 2. Typical SEM back-scattered electron images showing the microstructures of equilibrium phases obtained at 1250 °C; L-liquid phase.

Figure 3 shows the representative microstructures obtained at 1300 °C. Due to the limited experimental points, only the single liquid oxide phase and the three-phase equilibrium of liquid-rutile-pseudobrookite were observed. Sample E9 in Figure 3(a) displays a single phase with no observation of primary crystals. The white phase in Figure 3(b) was identified as rutile, and the light gray and dark gray matrix phases were designated as the pseudobrookite and quenched, glassy liquid oxide phase, respectively.

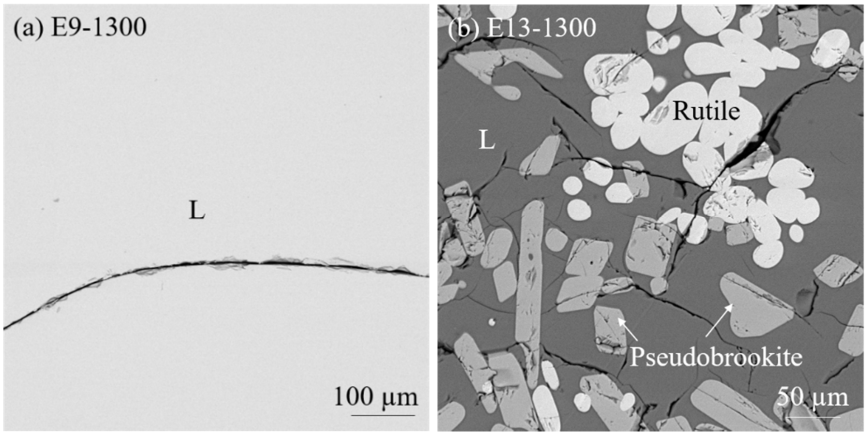

Fig. 3. Typical SEM back-scattered electron images showing the microstructures of equilibrium phases obtained at 1300 °C; L-liquid phase.

As for sample E13, it is interesting to observe that the liquid-rutile-pseudobrookite three-phase equilibria at 1300 °C was transformed into a two-phase equilibrium of liquid-pseudobrookite when the temperature was increased to 1400 °C. It can be seen in Figure 4(a) that the size of the pseudobrookite crystals precipitated in the primary phase field of pseudobrookite was relatively large (> 50μm), indicating that it is favorable for the application of the selective crystallization and phase separation (SCPS) method [12, 34]. An example of a single liquid oxide phase was found in sample E14 and is illustrated in Figure 4(b). A three-phase equilibrium was confirmed in sample E16 with the liquid oxide matrix coexisting with the rutile and pseudobrookite phases.

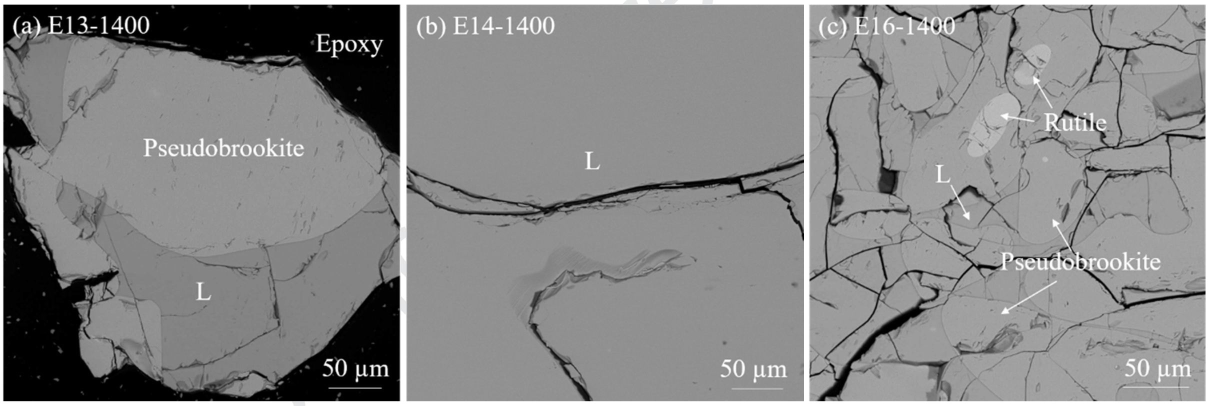

Fig. 4. Typical SEM back-scattered electron images showing the microstructures of equilibrium phases obtained at 1400 °C; L-liquid phase.

3.2 Comparison between experimental and computational results

As can be observed in Table 1, the MgO and Al_2O_3 contents in the liquid phase were approximately 8 wt% and 14 wt%, respectively. Due to the precipitation of MgO-containing crystals (i.e., the pseudobrookite solid solution) from the liquid phase of the system, the MgO and Al_2O_3 contents in the liquid phase of the quenched samples could not lie exactly on the designed contents of 10 wt% MgO and 15 wt% Al_2O_3, respectively. Therefore, the experimentally measured liquid compositions obtained at 1250-1400 °C in the present study were plotted onto the quasiternary CaO-SiO_2-TiO_2-14 wt% Al_2O_3-8 wt% MgO system, as shown in Figures 5-7. Based on the measured liquid compositions, the 1300 and 1400 °C isothermal sections were constructed.

The liquid composition was normalized before being depicted on the quasiternary phase diagram using the following steps: (1) the MgO and Al_2O_3 contents were recalculated to 8 wt% and 14 wt%, respectively; and (2) the total of CaO, SiO_2, and TiO_2 was normalized to 78 wt% with their original individual proportions. The experimental data from the literature [27, 29, 44, 45], the simulation results from FactSage [46] using the "FactPS" and "FToxid" databases, and from MTDATA [42, 43] with the MTOX database [43] were also projected onto the phase diagram for comparison.

Figure 5 shows the comparison of the present experimental results obtained at 1250 °C with the simulations by FactSage (Figure 5(a)) and MTDATA (Figure 5(b)). It was found that the liquidus domain measured experimentally by Shi et al. [27] agreed more consistently with the prediction by MTDATA, whereas the liquid phase domain simulated by FactSage was significantly larger, expanding toward the area with either a higher TiO_2 or SiO_2 content. The present results in the silica primary phase field were slightly on the higher side of the predictions by FactSage, shifting toward the SiO_2 corner. The 1250 °C liquidus domain obtained in the present study is significantly larger than the calculations by MTDATA, which show slightly too high liquidus contour temperatures for the feldspar primary phase field ($Al_2CaSi_2O_8$, the same phase as anorthite in FactSage) by only 15-25 °C compared with the present data.

Figure 6 shows the constructed 1300 °C isotherm based on the present experimentally measured liquid compositions. The results by Shi et al. [29] agree well with the data in the literature [44, 45]. The results in the perovskite primary phase field [29] fit well with the predictions by both FactSage and MTDATA. The 1300 °C isotherm constructed in the pseudobrookite primary phase field in the present study agrees well with the observations by Shi et al. [29], shifting slightly toward a higher TiO_2 content region when compared with the simulation by MTDATA. However, the pseudobrookite primary phase field was not observed in the calculations by FactSage, and the 1300 °C isotherm constructed according to the present results as well as the results by Shi et al. [29] shows a smaller liquid phase domain compared with the FactSage predictions.

The 1400 °C isotherm in Figure 7 obtained by Shi et al. [29] fits well with the predictions by FactSage and MTDATA in the perovskite primary phase field. However, the results obtained in the pseudobrookite primary phase field in the present study have significant discrepancies with the simulations. The present 1400 °C isotherm in the pseudobrookite primary phase field has a lower CaO content, compared with the prediction by MTDATA. To adjust the Ti-bearing slag composition based on the guideline of the phase diagram, further efforts are needed for accurate determination of the pseudobrookite primary phase field in the $CaO-SiO_2-TiO_2-Al_2O_3-MgO$ system.

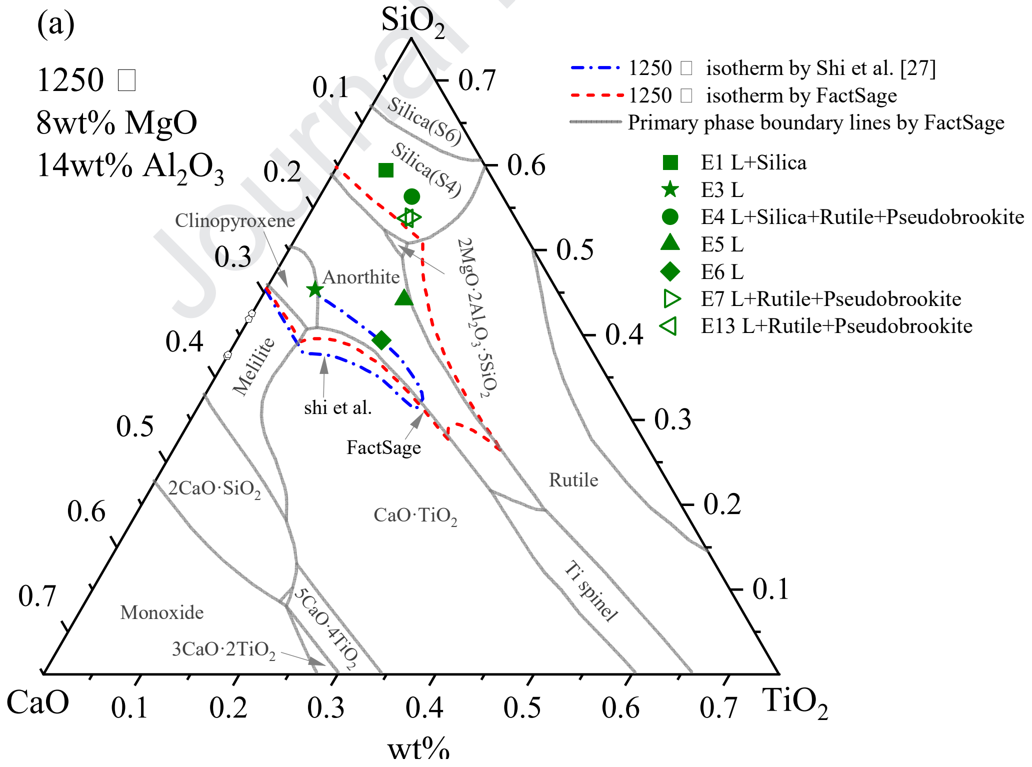

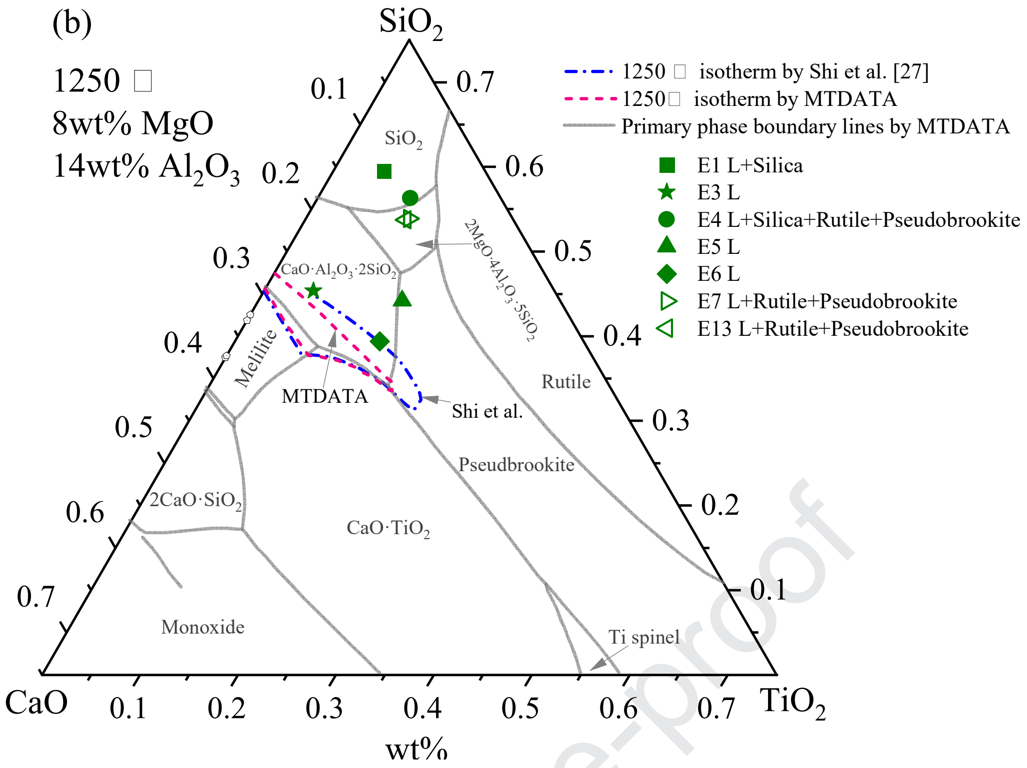

Fig. 5. A comparison of the equilibrium liquid domain compositions obtained at 1250 °C with the simulations by FactSage (a) and MTDATA (b) superimposed; $CaO·Al_2O_3·2SiO_2$-feldspar, the same phase as anorthite in FactSage.

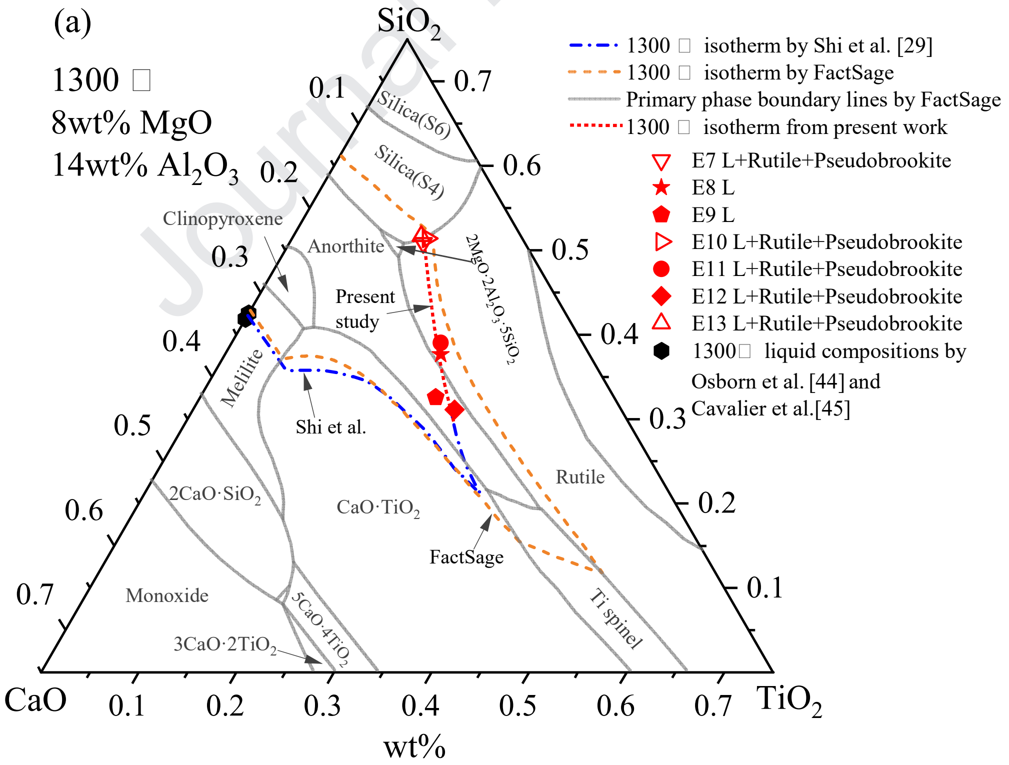

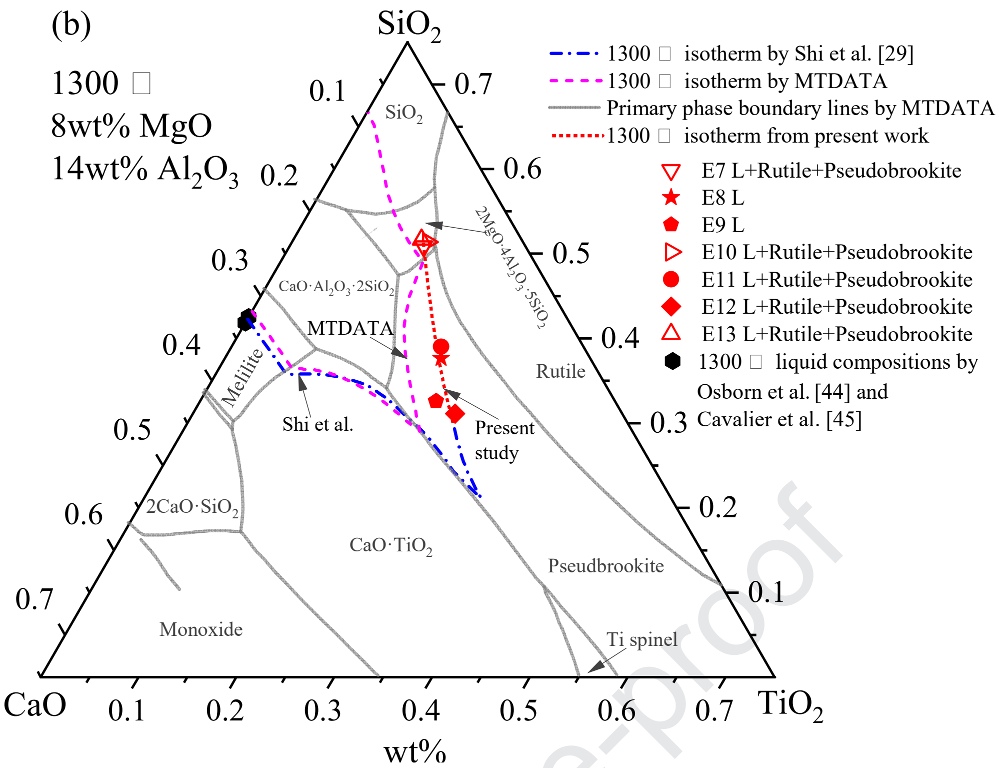

Fig. 6. A comparison of the equilibrium liquid domain compositions obtained at 1300 °C with the simulations by FactSage (a) and MTDATA (b) superimposed.

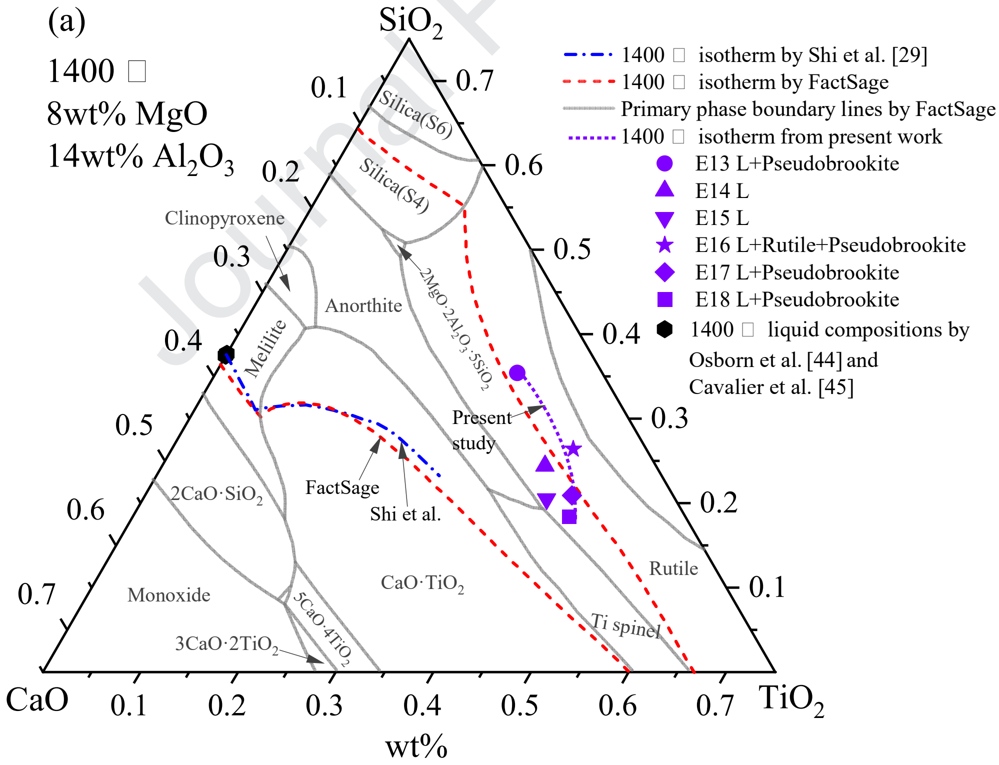

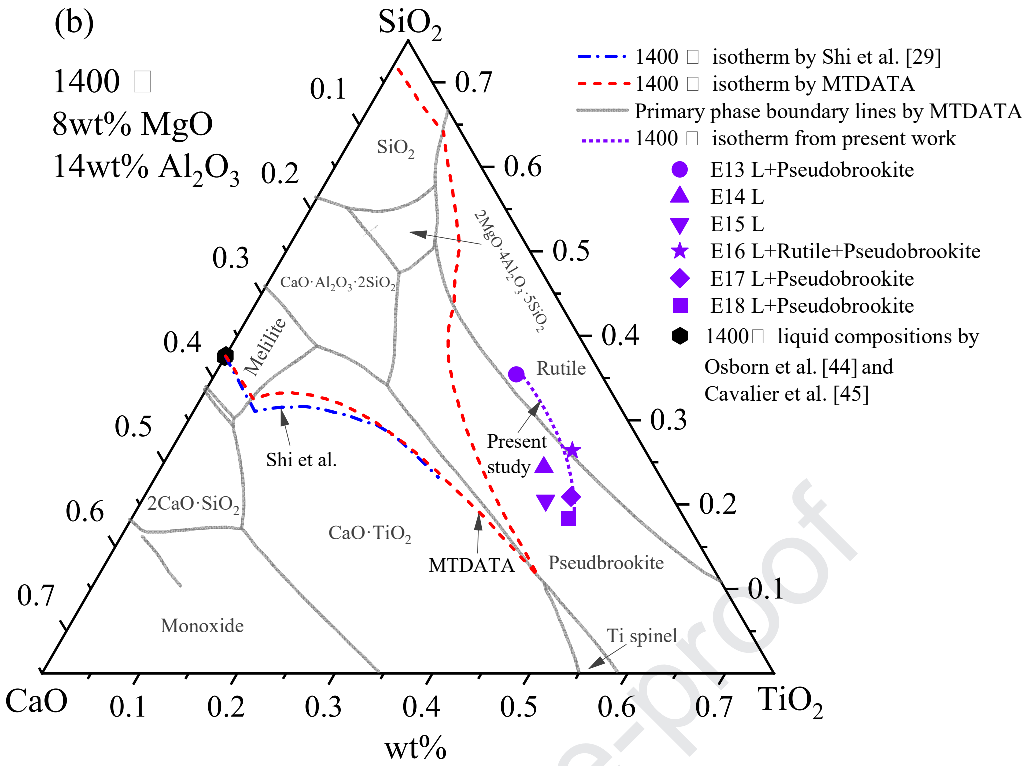

Fig. 7. A comparison of the equilibrium liquid domain compositions obtained at 1400 °C with the simulations by FactSage (a) and MTDATA (b) superimposed.

4. Conclusions and Summary

The phase relations of the $CaO-SiO_2-TiO_2-Al_2O_3-MgO$ system at 1250-1400 °C were experimentally investigated in equilibrium with air using the high-temperature equilibration/quenching/SEM-EDS in situ phase analysis method. The silica primary phase, rutile primary phase, and pseudobrookite solid solution primary phase were observed. Based on the current experimental results as well as the data from the literature, 1300 and 1400 °C $CaO-SiO_2-TiO_2$-14 wt% Al_2O_3-8 wt% MgO quasiternary phase diagram isotherms were constructed, which will serve as guidelines for the slag composition optimization by adding slag modifiers or adjusting temperature for selective crystallization of pseudobrookite solid solution and recovery of titania from slag. The present results provide fundamental information for further systematic study on the phase relations of titania-bearing slag systems.

Acknowledgments

This work was partly financed by the Aalto University School of Chemical Engineering. The Academy of Finland's RawMatTERS Finland Infrastructure (RAMI) based at Aalto University, GTK Espoo, and VTT Espoo was utilized in this study. The authors are grateful to the China Scholarship Council for financial support [grant number 201806370217].

References

[1]. Zhang, W., Zhang, L., Li, Y., & Li, X. (2015). An environmental procedure to extract titanium components and metallic iron from Ti-bearing blast furnace slag. *Green Processing and Synthesis*, 4(4), 307-316. https://doi.org/10.1515/gps-2015-0031

[2]. Zhang, L., Zhang, W., Zhang, J., & Li, G. (2016). Oxidation kinetics and oxygen capacity of Ti-bearing blast furnace slag under dynamic oxidation conditions. *Metals*, 6(5), 105. https://doi.org/10.3390/met6050105

[3]. Ren, S., Zhao, Q., Yao, L., & Liu, Q. (2016). Precipitation behavior of perovskite and anosovite crystals from high Ti-bearing blast furnace slag with small amount of B_2O_3. *Cryst. Eng. Comm*, 18(8), 1393-1402. https://doi.org/10.1039/C5CE02131F

[4]. Han, J., Zhang, J., Zhang, J., Chen, X., Zhang, L., & Tu, G. (2020). Combined effect of SiO_2 and O_2 on the

crystallization behavior of modified Ti-bearing blast furnace slag. *ACS Omega.* 5(15), 8619-8628. https://doi.org/10.1021/acsomega.0c00014

[5]. Wu, Z., Li, Z., Ju-hua, Z., & Nai-Xiang, F. (2012). Crystallization and coarsening kinetics of rutile phase in modified Ti-bearing blast furnace slag. *Industrial & Engineering Chemistry Research*, 51(38), 12294-12298. https://doi.org/10.1021/ie3007825

[6]. Lou, T. P., Li, Y. H., Li, L., & Sui, Z. (2000). Study of precipitation of perovskite phase from the oxide slag. *Acta Metallurgica Sinica-Chinese Edition*, 36(2), 141-144.

[7]. Zhang, L., Zhang, L. N., Wang, M. Y., Li, G. Q., & Sui, Z. T. (2007). Recovery of titanium compounds from molten Ti-bearing blast furnace slag under the dynamic oxidation condition. *Minerals Engineering*, 20(7), 684-693. https://doi.org/10.1016/j.mineng.2007.01.003

[8]. Li, J., Zhang, Z., Zhang, M., Guo, M., & Wang, X. (2011). The influence of SiO_2 on the extraction of Ti element from Ti‐bearing blast furnace slag. *Steel Research International*, 82(6), 607-614. https://doi.org/10.1002/srin.201000217

[9]. Li, J., Wang, X., & Zhang, Z. (2011). Crystallization behavior of rutile in the synthesized Ti-bearing blast furnace slag using single hot thermocouple technique. *ISIJ International*, 51(9), 1396-1402. https://doi.org/10.2355/isijinternational.51.1396

[10]. Zhao, Q., Liu, C. J., Cao, L. H., Jiang, M. F., Li, B. K., Saxén, H., & Zevenhoven. R. (2019). Shear-force based stainless steel slag modification for chromium immobilization. *ISIJ International*, 59, 583-589. https://doi.org/10.2355/isijinternational.ISIJINT-2017-678

[11]. Zhang, W., Zhang, L., Zhang, J. H., & Feng, N. X. (2013). Effect of oxidation on phase transformation in Ti-bearing blast furnace slag. *Advanced Materials Research*, 641, 363-366. https://doi.org/10.4028/www.scientific.net/AMR.641-642.363

[12]. Wang, Z., Liu, X., Zhang, L., & Zhu, Q. (2016). The influence of composition on crystallization and liberation behavior of Ti-rich phase in Ti-bearing slags. *Transactions of the Indian Institute of Metals*, 69(1), 97-105. https://doi.org/10.1007/s12666-015-0720-8

[13]. Sun, L., Shi, J., Yu, Z., & Jiang, M. (2019). Phase equilibria and liquidus surface of CaO-SiO_2-5 wt% MgO-Al_2O_3-TiO_2 slag system. *Ceramics International*, 45(1), 481-487. https://doi.org/10.1016/j.ceramint.2018.09.193

[14]. Goso X., Nell J., Petersen J. (2016) Review of liquidus surface and phase equilibria in the TiO_2-SiO_2-Al_2O_3-MgO-CaO slag system at PO_2 applicable in fluxed titaniferous magnetite smelting. In: Reddy R.G., Chaubal P., Pistorius P.C., Pal U. (eds) Advances in Molten Slags, Fluxes, and Salts: *Proceedings of the 10th International Conference on Molten Slags, Fluxes and Salts 2016*. Springer, Cham, pp. 105-114. https://doi.org/10.1007/978-3-319-48769-4_11

[15]. Li, Y., Lou, T., Xia, Y., & Sui, Z. (2000). Kinetics of non-isothermal precipitation process of the perovskite phase in CaO-TiO_2-SiO_2-Al_2O_3-MgO system. *Journal of Materials Science*, 35(22), 5635-5637. https://doi.org/10.1023/A:1004885819661

[16]. Liu, L., Hu, M., Bai, C., Lv, X., Wen, L., & Zhang, S. (2014). In situ observation of the crystallisation process of perovskite in titanium-bearing blast furnace slag. *Mineral Processing and Extractive Metallurgy*, 123(4), 241-245. https://doi.org/10.1179/1743285514Y.0000000079

[17]. Gao J. T., Li J. C., & Guo Z. C. (2014). Separation of perovskite phase from CaO-TiO_2-SiO_2-Al_2O_3-MgO system by supergravity. In: *5th International Symposium on High-Temperature Metallurgical Processing* ed. Tao Jiang and Joseph Lessard (San Diego, CA: TMS, 2014), pp. 67-72.

[18]. Li, J. C., Guo, Z. C., & Gao, J. T. (2014). Isothermal enriching and separation of perovskite phase from CaO-TiO_2-SiO_2-Al_2O_3-MgO melt by centrifugal force. *Ironmaking & Steelmaking*, *41*(10), 776-783. https://doi.org/10.1179/1743281214Y.0000000206

[19]. Wang, M. Y., Zhang, L. N., Zhang, L., Sui, Z. T., & Tu, G. F. (2006). Selective enrichment of TiO_2 and precipitation behavior of perovskite phase in titania bearing slag. *Transactions of Nonferrous Metals Society of China*, 16(2), 421-425. https://doi.org/10.1016/S1003-6326(06)60072-1

[20]. Li, Y. H., Lou, T. P., & Sui, Z. T. (2000). Effects of CaO and MnO on the crystallization of the perovskite phase in the Ti-bearing blast furnace slag. *Journal of Iron and Steel Research*, 12(3), 1-4.

[21]. Taiping, L., Yuhai, L., Liaosha, L., & Zhitong, S. (2000). Study on kinetics of perovskite phase precipitate in slag bearing titanium. *Journal of the Chinese Ceramic Society*, 28(3), 255-258.

[22]. Gao, J., Lu, Y., Wang, F., & Guo, Z. (2017). Effects of super-gravity field on precipitation and growth kinetics of perovskite crystals in CaO-TiO_2-SiO_2-Al_2O_3-MgO melt. *Ironmaking & Steelmaking*, 44(9), 692-698. https://doi.org/10.1080/03019233.2016.1228740

[23]. Zhang, L., Zhang, L. N., Wang, M. Y., Lou, T. P., Sui, Z. T., & Jang, J. S. (2006). Effect of perovskite phase precipitation on viscosity of Ti-bearing blast furnace slag under the dynamic oxidation condition. *Journal of Non-crystalline Solids*, 352(2), 123-129. https://doi.org/10.1016/j.jnoncrysol.2005.11.012

[24]. Fu, N. X., Zhang, L., Cao, H. Y., & Sui, Z. T. (2008). Effects of additives on precipitation behavior of perovskite in Ti-Bearing blast furnace slag. *Journal of Iron and Steel Research*, 20(4), 13.

[25]. Wang, Z., Sun, H. Y., & Zhu, Q. S. (2019). Effects of the continuous cooling process conditions on the crystallization and liberation characteristics of anosovite in Ti-bearing titanomagnetite smelting slag. *International Journal of Minerals, Metallurgy, and Materials*, 26(9), 1120-1128. https://doi.org/10.1007/s12613-019-1830-9

[26]. Wang, Z., Zhu, Q., & Sun, H. (2019). Phase equilibria in the TiO_2-rich part of the TiO_2-CaO-SiO_2-10 Wt Pct Al_2O_3-5 Wt Pct MgO system at 1773 K. *Metallurgical and Materials Transactions B*, 50(1), 357-366. https://doi.org/10.1007/s11663-018-1441-2

[27]. Shi, J., Chen, M., Santoso, I., Sun, L., Jiang, M., Taskinen, P., & Jokilaakso, A. (2020). 1250 °C liquidus for the CaO-MgO-SiO_2-Al_2O_3-TiO_2 system in air. *Ceramics International*, 46(2), 1545-1550. https://doi.org/10.1016/j.ceramint.2019.09.122

[28]. Shi, J., Sun, L., Qiu, J., & Jiang, M. (2018). Phase equilibrium investigation for CaO-SiO_2-5wt.% MgO-20wt.% Al_2O_3-TiO_2 system relevant to Ti-bearing slag system. *ISIJ International*, 58(3), 431-438. https://doi.org/10.2355/isijinternational.ISIJINT-2017-555

[29]. Shi, J., Chen, M., Wan, X., Taskinen, P., & Jokilaakso, A. (2020). Phase equilibrium study of the CaO-SiO_2-MgO-Al_2O_3-TiO_2 system at 1300 °C and 1400 °C in air. *JOM*. https://doi.org/10.1007/s11837-020-04136-1

[30]. Shi, J., Sun, L., Qiu, J., & Jiang, M. (2017). Phase equilibria of CaO-SiO_2-5wt.% MgO-30 wt.% Al_2O_3-TiO_2 system at 1400 °C and 1450 °C relevant to high Al_2O_3 Ti-bearing blast furnace slag system. *Journal of Alloys and Compounds*, 722, 25-32. https://doi.org/10.1016/j.jallcom.2017.06.058

[31]. Shi, J., Sun, L., Zhang, B., Liu, X., Qiu, J., Wang, Z., & Jiang, M. (2016). Experimental determination of the phase diagram of the CaO-SiO_2-5 pctMgO-10 pctAl_2O_3-TiO_2 system. *Metallurgical and Materials Transactions B*, 47(1), 425-433. https://doi.org/10.1007/s11663-015-0527-3

[32]. Shi, J., Sun, L., Qiu, J., Wang, Z., Zhang, B., & Jiang, M. (2016). Experimental determination of the phase diagram for CaO-SiO_2-MgO-10% Al_2O_3-5% TiO_2 system. *ISIJ International*, 56(7), 1124-1131. https://doi.org/10.2355/isijinternational.ISIJINT-2016-045

[33]. Sun, L., Shi, J., Liu, C., & Jiang, M. (2019). Phase equilibria studies for CaO-SiO_2-5wt.% MgO-Al_2O_3-TiO_2 system in high Al_2O_3 content area with w (CaO)/w (SiO_2) ratio of 1.50. *Journal of Alloys and Compounds*, 810, 151949. https://doi.org/10.1016/j.jallcom.2019.151949

[34]. Sun, L., Shi, J., Yu, Z., & Jiang, M. (2019). Phase equilibria and liquidus surface of CaO-SiO_2-5 wt% MgO-Al_2O_3-TiO_2 slag system. *Ceramics International*, 45(1), 481-487. https://doi.org/10.1016/j.ceramint.2018.09.193

[35]. Sun, L. F., Shi, J. J., Zhang, B., Qiu, J. Y., Wang, Z. Y., & Jiang, M. F. (2017). Liquidus and phase equilibria in CaO-SiO_2-5% MgO-20% Al_2O_3-TiO_2 system. *Journal of Central South University*, 24(1), 48-55. https://doi.org/10.1007/s11771-017-3407-y

[36]. Osborn, E. F., & Gee, K. H. (1969). Phase equilibria at liquidus temperatures for a part of the system CaO-MgO-Al_2O_3-TiO_2-SiO_2 and their bearing on the effect of titania on the properties of blast furnace slag. *Bull. Earth and Mineral Sciences Experiment Station*, No. 85, 57-80.

[37]. Zhao, B., Jak, E., & Hayes, P. C. (2009). Phase equilibria studies in the slag system "TiO_2"-CaO-MgO-Al_2O_3-SiO_2 at carbon saturation. In: *VIII International Conference on Molten Slags, Fluxes and Salts*, Santiago, Chile. ChIMM, Santiago, pp. 71-82.

[38]. Jak, E., & Hayes, P. C. (2008). Phase equilibria determination in complex slag systems. *Mineral Processing and Extractive Metallurgy*, 117(1), 1-17. https://doi.org/10.1179/174328508X272344

[39]. Chen, M., Avarmaa, K., Klemettinen, L., O'Brien, H., Sukhomlinov, D., Shi, J., Taskinen, P., & Jokilaakso, A. (2020). Recovery of precious metals (Au, Ag, Pt, and Pd) from urban mining through copper smelting.

Metallurgical and Materials Transactions B, 1-14. https://doi.org/10.1007/s11663-020-01861-5

[40]. Chen, M., Shi, J., Taskinen, P., & Jokilaakso, A. (2020). Experimental determination of the 1300 °C and 1400 °C isotherms for CaO-SiO_2-TiO_2-10 wt% Al_2O_3 system in air. *Ceramics International*, 46(7), 9183-9191. https://doi.org/10.1016/j.ceramint.2019.12.170

[41]. Bastin, G. F., Dijkstra, J. M., & Heijligers, H. J. M. (1998). PROZA96: an improved matrix correction program for electron probe microanalysis, based on a double Gaussian φ (ρz) approach. *X□Ray Spectrometr*y, 27(1), 3-10. https://doi.org/10.1002/(SICI)1097-4539(199801/02)27:1<3::AID-XRS227>3.0.CO;2-L

[42]. Davies, R. H., Dinsdale, A. T., Gisby, J. A., Robinson, J. A. J., Martin, & A. M. (2002). MTDATA-thermodynamic and phase equilibrium software from the national physical laboratory. *Calphad*, 26(2), 229-271. https://doi.org/10.1016/S0364-5916(02)00036-6

[43]. Gisby, J., Taskinen, P., Pihlasalo, J., Li, Z., Tyrer, M., Pearce, J., Avarmaa, K., Björklund, P., Davies, H., Korpi, M., Martin, S., Pesonen, L., & Robinson, J. (2017). MTDATA and the prediction of phase equilibria in oxide systems: 30 years of industrial collaboration. *Metallurgical and Materials Transactions B*, 48(1), 91-98. https://doi.org/10.1007/s11663-016-0811-x

[44]. Osborn, E. F., DeVries, R. C., Gee, K. H., & Kraner, H. M. (1954). Optimum composition of blast furnace slag as deduced from liquidus data for the quaternary system CaO-MgO-Al_2O_3-SiO_2. *JOM*, 6(1), 33-45. https://doi.org/10.1007/BF03397977

[45]. Cavalier, G., & Sandrea-Deudon, M. (1960). Laitiers quaternaires CaO-MgO-Al_2O_3-SiO_2: température de cristallisation commençante et champs de cristallisation sur plans a magnésie constante. Revue de Métallurgie, 57(12), 1143-1157.

[46]. Bale, C. W., Bélisle, E., Chartrand, P., Decterov, S. A., Eriksson, G., Hack, K., Jung, I.-H., Kang, Y.-B., Melançon, J., Pelton, A.D., Robelin. C., & Petersen, S. (2009). FactSage thermochemical software and databases-recent developments. *Calphad*, 33(2), 295-311. https://doi.org/10.1016/j.calphad.2008.09.009

Declaration of interests

☒ The authors declare that they have no known competing financial interests or personal relationships that could have appeared to influence the work reported in this paper.

☐The authors declare the following financial interests/personal relationships which may be considered as potential competing interests: